

## 27. CHINOOK TROUGH RIFTING AND HYDROTHERMAL DEPOSITION AT SITES 885 AND 886<sup>1</sup>

Gerald R. Dickens<sup>2</sup> and Robert M. Owen<sup>2</sup>

### ABSTRACT

The Chinook Trough is a pronounced deep located in the central North Pacific Ocean that spans approximately 1500 km in a northeast-southwest direction. Geophysical and geomorphological considerations suggest that this feature is the southern lithospheric scar marking initiation of Late Cretaceous north-south rifting within the ancient Farallon Plate. If this hypothesis is correct, then, by analogy to other active and passive mid-ocean rift zones, Late Cretaceous sediment deposited immediately south of the Chinook Trough should contain significant amounts of hydrothermal material deposited in association with the intraplate rifting event. Because the proposed tectonic origin for the Chinook Trough places seafloor south of the eastern end of the trough beneath the Cretaceous calcite compensation depth (CCD), expected hydrothermal components deposited during the Late Cretaceous at these locations also should lack carbonate dilution.

Ocean Drilling Program Sites 885 and 886 were drilled approximately 60 km south of the northeast section of the Chinook Trough. High-resolution chemical and mineralogical analyses demonstrate that sediment deposited after 75–81 Ma at these sites contains an extensive record of hydrothermal deposition without associated carbonate. Various proxy indicators suggest that the flux of hydrothermal material decreases in a roughly exponentially pattern upcore and reaches background levels in the early Paleogene. Lowermost sediment is similar in composition to that of Neogene and Holocene distal hydrothermal sediment deposited along the East Pacific Rise and is characterized as follows: (1) a primary mineralogy of poorly crystalline goethite, amorphous Fe-Mn oxyhydroxides, and apatite; (2) bulk sediment Fe concentrations between 23.5% and 32.5%; (3) bulk concentrations of As, Mo, Sb, and Zn that are 1–2 orders of magnitude higher than “normal” biogenic-free pelagic sediment; and (4) a pronounced bulk Ce-anomaly. These results are consistent with the hypothesis that the Chinook Trough represents onset of north-south Late Cretaceous rifting, and they provide a detailed record of hydrothermal deposition emanating from an intraplate spreading center.

### INTRODUCTION

Our present understanding of the tectonic evolution of the Pacific during the Late Cretaceous primarily hinges upon geologic interpretations of large topographic features (e.g., Rea and Duncan, 1986; Mammerickx and Sharman, 1988; Atwater et al., 1993). One such feature is the Chinook Trough, a pronounced deep in the central north Pacific that extends approximately 1500 km in an northeast-southwest direction. Several investigations (Erickson et al., 1969; Rea, 1970; Woods and Davies, 1982; Rea and Dixon, 1983; Mammerickx and Sharman, 1988; Atwater et al., 1993) of the general seafloor geology in this region have suggested that the trough is a lithospheric scar that formed during the Late Cretaceous and subsequently was “left behind” as a newly created east-west spreading center moved northward.

Reconstructions of ancient rifting events have shown that such events may be recorded as a dramatic increase in the flux of hydrothermal materials to sediment deposited within a few hundred kilometers of the rifting center, presumably resulting from an increase in hydrothermal circulation during rifting (Lyle et al., 1986, 1987; Owen and Zimmerman, 1991). Consequently, a primary objective for drilling at Ocean Drilling Program (ODP) Sites 885 and 886 was to seek independent corroborative evidence in support of the rifting hypothesis by documenting the existence of a characteristic record of hydrothermal materials in the sediment column immediately south of the Chinook Trough (Rea, Basov, Janecek, Palmer-Julson, et al., 1993). Here we present chemical and mineralogical results from sediment deposited at Sites 885 and 886 that are in accord with the view that Chinook Trough is a remnant feature of a Late Cretaceous intraplate rifting episode.

### BACKGROUND

#### The Chinook Trough

The Chinook Trough (Figs. 1, 2) comprises a series of discrete east-trending segments that span approximately 1500 km from the Emperor Trough (41.5°N, 179.0°E) to the axis of the Great Magnetic Bight (45.2°N, 166.0°W; Rea and Dixon, 1983). The trough is topographically expressed as a prominent deep with vertical relief commonly between 1500 and 2000 m and a maximum depth of 7140 m below sea level (mbsl; Rea, 1970; Rea and Dixon, 1983).

Geophysical and geomorphological observations (e.g., Erickson et al., 1969; Rea, 1970; Woods and Davies, 1982; Rea and Dixon, 1983; Mammerickx and Sharman, 1988; Atwater et al., 1993) pertinent to understanding the origin of the Chinook Trough include the following: (1) magnetic lineations north of the trough decrease in age away from the Chinook Trough; (2) the spatial orientation of magnetic lineations north of the trough roughly parallels the Chinook Trough; (3) fracture zones north of the trough (e.g., Adak and Amlia) end at the Chinook Trough; (4) the axis of the Great Magnetic Bight coincides with the eastern edge of the Chinook Trough; and (5) tectonic spreading fabrics suggest north-south seafloor spreading north of the trough, but east-west spreading south of the trough. Based upon these observations, the Chinook Trough has been interpreted as representing a scarp that marks initiation of intraplate rifting within the ancient Farallon Plate and onset of north-south seafloor spreading between the Pacific Plate and the now subducted Kula Plate (Fig. 3). Thus, the Chinook Trough is analogous to scarps presently bounding the East Pacific Rise (Sclater et al., 1971; Rea, 1981; Cande et al., 1982), except that both the parallel scarp and the ancient Kula-Pacific spreading ridge have been subducted to the north into the present Aleutian Trench.

Further inferences regarding rifting and Kula-Pacific spreading can be hypothesized from maps of magnetic lineations north of the Chinook Trough. First, the Chinook Trough transects Chrons 33R and 34 such that the northeast end of the trough is younger than the southwest end (Mammerickx and Sharman, 1988; Atwater et al.,

<sup>1</sup> Rea, D.K., Basov, I.A., Scholl, D.W., and Allan, J.F. (Eds.), 1995. *Proc. ODP, Sci. Results*, 145: College Station, TX (Ocean Drilling Program).

<sup>2</sup> Department of Geological Sciences, University of Michigan, Ann Arbor, MI 48109-1063, U.S.A.

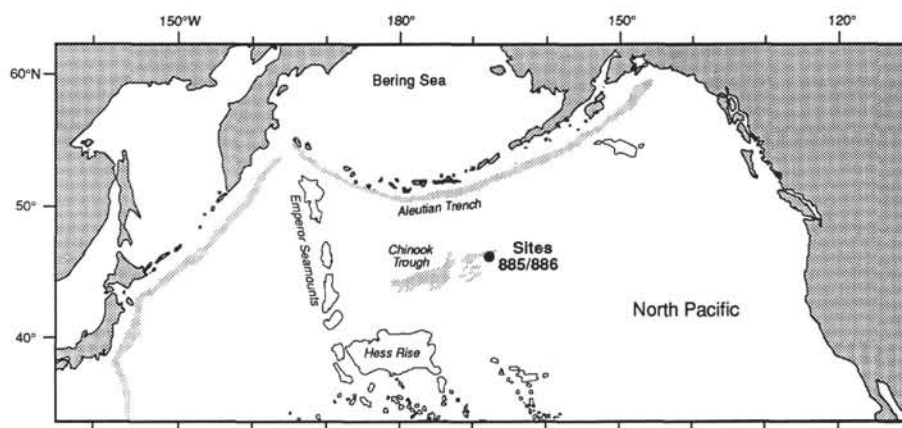


Figure 1. Location of the Chinook Trough and Sites 885 and 886 in the central North Pacific. Sites 885 and 886 are proximal (2 km apart) and lie approximately 60 km south of the northeast end of the Chinook Trough.

1993). This suggests that the Chinook Trough propagated from west to east (Atwater et al., 1993). Applying the time scale of Cande and Kent (1992), this also implies that later stages of rifting (at the northeast end) occurred between 79 and 83 Ma (Atwater et al., 1993). Second, distances between magnetic isochrons indicate two distinct regimes of spreading existed during the Late Cretaceous–early Paleogene. The rough topography immediately north of the Chinook Trough formed during relatively slow half spreading rates (0–1.8 cm/yr; Mammerickx and Sharman, 1988), whereas the smoother topography to the north formed during relatively rapid half spreading rates (3.5–4.4 cm/yr; Rea and Dixon, 1982; Woods and Davies, 1983; Mammerickx and Sharman, 1988). Mammerickx and Sharman (1988) have estimated that the jump in spreading rate (and change in topography) occurred at approximately 75.3 Ma. Using the magnetic isochron map of Atwater et al. (1993) and the revised time scale of Cande and Kent (1992), the age of this transition may be slightly younger (~74.5 Ma). Third, by analogy with the present-day relationship between spreading rate and ridge topography, the shape of the Kula-Pacific Ridge likely changed around 75 Ma. Present-day ridges that exhibit relatively slow spreading (half spreading rates < 2.5 cm/yr) typically have a prominent axial valley, whereas relatively rapid spreading ridges (half spreading rates > 3 cm/yr) generally lack such a valley (e.g., Kennett, 1982).

### Geochemical Record of Rifting Events

Previous investigations have shown that both active and passive (Sengor and Burke, 1978) rifting events are recorded as significant increases in the flux of hydrothermal materials to sediment in the region (i.e., within a few hundred kilometers) of the rifting center, probably because hydrothermal circulation substantially increases after fracturing of oceanic crust provides seawater with access to deep-seated heat sources (Owen and Rea, 1985; Lyle et al., 1986, 1987; Owen and Zimmerman, 1991). Hydrothermal fluids emanating from vents at modern active seafloor spreading centers are enriched by more than an order of magnitude in certain metals (e.g., Fe, Mn, Ba, Zn, REEs) relative to seawater (e.g., Michard et al., 1983; Von Damm et al., 1985; Fouquet et al., 1991). Although a portion of these metals is precipitated adjacent to vents, significant quantities enter neutrally buoyant plumes, which can be traced laterally over great distances when they emanate from ridges without prominent axial valleys (Lupton et al., 1980; Baker et al., 1985; Klinkhammer and Hudson, 1986; German et al., 1991). The formation of oxyhydroxide particulates within such plumes, and the slow settling of these phases onto the underlying seafloor, deposit metal-rich sediment within hundreds of kilometers from active “Pacific-like” spreading centers (e.g., Boström et al., 1969; Dymond, 1981; Lyle et al., 1986). Here we classify such metalliferous sediment as “distal hydrothermal sedi-

ment” to distinguish it from more proximal hydrothermal deposits (e.g., mounds, crusts, and chimneys).

Distal hydrothermal sediments exhibit several compositional characteristics, which serve to identify them and to discriminate them from other types of hydrogenous deposits. These characteristics include (e.g., Meylan et al., 1981; Barrett et al., 1988): (1) extremely high concentrations of Fe and Mn, which exist in various oxyhydroxide minerals and amorphous oxyhydroxide phases; (2) abundant apatite; (3) significantly elevated concentrations of certain trace metals (e.g., As, Ni, Mo, Sb, V, and Zn); (4) notably low concentrations of Co relative to other types of ferromanganese deposits; (5) low bulk concentrations of lithophile elements (e.g., Al and Sc); and (6) a pronounced negative Ce anomaly. The latter observation is valid despite the fact that REE patterns of hydrothermal solutions display no Ce anomaly (Michard et al., 1983); hydrothermally derived Fe-Mn oxyhydroxides rapidly scavenge REEs from seawater such that distal hydrothermal precipitates have a Ce-depleted REE pattern similar to that of seawater (Ruhlin and Owen, 1986; German et al., 1990).

Another noteworthy characteristic of distal hydrothermal sediment is that its accumulation rate decreases in a roughly exponential pattern with increasing distance from the ridge crest (Boström et al., 1969; Dymond, 1981; Lyle et al., 1986, 1987; Marchig and Erzinger, 1986). Lyle et al. (1986) have suggested that this pattern arises because of the combined effects of the particle size distribution injected at vents, advective transport of hydrothermal precipitates within the plume, and precipitate settling rates. Thus, as a piece of seafloor moves away from an active spreading center, the lateral distribution of hydrothermal precipitates is manifested as an exponential decrease in the flux of distal hydrothermal sediment upcore. A roughly exponential decrease of distal hydrothermal deposition with increasing distance from the paleoridge crest ridge has been observed in Neogene sediment deposited along the East Pacific Rise (Lyle et al., 1986; Marchig and Erzinger, 1986). In addition, such studies show the occasional occurrence of deviations from the expected accumulation pattern in the form of prominent “spikes” of hydrothermal materials. Lyle et al. (1987) have suggested that these deviations are correlative with pulsations in the intensity of hydrothermal activity resulting from tectonic reorganizations, such as ridge jumps and/or changes in ridge orientation.

### SITE AND SAMPLE DESCRIPTION

Sites 885 (44°41'N, 168°16'W) and 886 (44°41'N, 168°14'W) are proximal (within 2.2 km) and located approximately 60 km south of the northeastern end of the Chinook Trough (Fig. 1) at water depths ranging from 5713 to 5778 m. Drilling at these sites recovered approximately 72 m of sediment, which has been divided into three basic lithologic units (Rea, Basov, Janeczek, Palmer-Julson, 1993): a

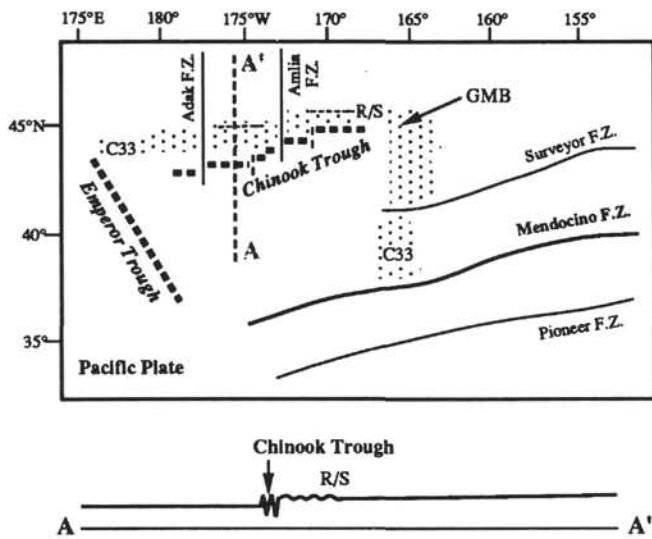


Figure 2. The Chinook Trough is a pronounced deep in the central North Pacific that spans approximately 1500 km in a northeast-southwest direction. The trough is bounded to the west by the Emperor Trough and to the east by the Great Magnetic Bight (GMB). The southern end of two major fracture zones—the Adak and Amlia—transect the Chinook Trough into a series of discrete east-trending segments. Vertical relief across these segments commonly exceeds 1500 m (Rea and Dixon, 1983). Magnetic Anomaly 33 (C33) is shaded to show that the Chinook Trough transects this anomaly (Atwater et al., 1993). Other magnetic anomalies north of the trough are roughly parallel to the Chinook Trough, and decrease in age with increasing distance from the trough. Topography immediately north of the Chinook Trough is characterized by abyssal hills that end at a “rough/smooth” (R/S) boundary (Mammerickx and Sharman, 1988). F.Z. = fracture zone.

late Pliocene to Pleistocene unit of reddish brown clay with diatoms (Unit I); a late Miocene to late Pliocene unit of light brown diatom ooze with clay (Unit II); and a late Miocene to older unit of clay with oxyhydroxides (Unit III). The color of Unit III grades from yellowish brown to very dark brown with increasing depth (Rea, Basov, Janecek, Palmer-Julson, 1993). Biogenic silica is notably absent in the lower depths (>56 mcd) of Unit III; carbonate was below detection limits in samples from all three units (Rea, Basov, Janecek, Palmer-Julson, 1993). Aphyric basalt (Unit IV) without baked contacts underlies the third lithologic unit.

Total organic carbon (TOC) concentrations for all three lithologic units are very low, with TOC ranging between 0.02% and 0.25% and typically less than 0.10% (Rea, Basov, Janecek, Palmer-Julson, 1993). Titration alkalinity is also low (2.49 to 2.74 mM) within pore waters at Sites 885 and 886 (Rea, Basov, Janecek, Palmer-Julson, 1993). Dissolved  $\text{SO}_4^{2-}$  concentrations range from 27.1 to 28.8 mM and are similar to that of North Pacific deep water (Rea, Basov, Janecek, Palmer-Julson, 1993). These data and the overall reddish brown coloring suggest that sediment sequences at Sites 885 and 886 are well oxidized and that extensive postdepositional metal remobilization has not occurred. If elevated TOC, alkalinity, and/or depleted  $\text{SO}_4^{2-}$  were found, metal oxide reduction of organic matter likely would have been an important sedimentary process (e.g., Froelich et al., 1979; Rabouille and Gaillard, 1991). Pore-water Mn and  $\text{NH}_4^+$  profiles may indicate that some degree of suboxic diagenesis and Mn remobilization has occurred within lithologic Unit II (Rea, Basov, Janecek, Palmer-Julson, 1993); however, the presence of round, concentrically banded Mn nodules of nondiagenetic origin near the Unit II/III boundary (Rea, Basov, Janecek, Palmer-Julson, 1993) demonstrates that postdepositional Mn remobilization was not a significant process in deeper sediment. Because Mn is more redox sensitive than Fe and most other transition metals (e.g., Froelich et al., 1979), we

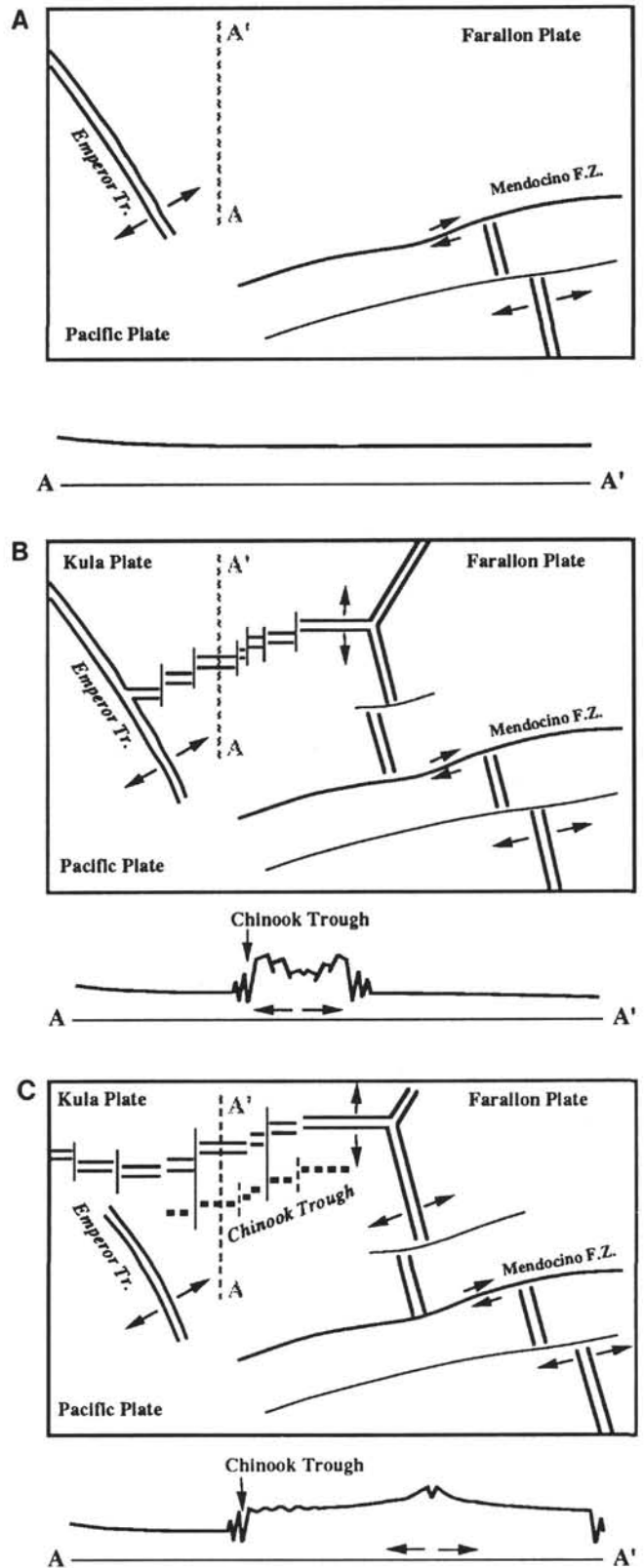


Figure 3. Tectonic evolution of the Chinook Trough (from Rea and Dixon, 1983; Atwater et al., 1993). **A.** Prerifting: two major plates (Pacific and Farallon) existed in this region of the Pacific. **B.** Rifting: intraplate rifting was initiated within the ancient Farallon Plate and created the Kula-Pacific Spreading Ridge. **C.** Postrifting: the Chinook Trough represents one of two scarps formed during rifting. The parallel scarp as well as the Kula-Pacific Spreading Ridge have now been subducted. F.Z. = fracture zone.

infer that significant metal remobilization has not occurred in sediment deposited before the late Miocene (i.e., Unit III).

This study involved the mineralogical, electron microscopic, and chemical analyses of bulk sediment samples from lithologic Unit III at Holes 885A, 886B, and 886C. Individual samples represent 5-cm intervals from Sections 145-885A-6H-2 through -6H-7 (44.15–51.53 mbsf), Sections 145-886B-7H-2 through -7H-CC (50.85–59.04 mbsf), and Sections 145-886C-7H-1 through -8H-6 (54.35–72.10 mbsf). It is clear that downcore depths within these three holes are offset; hence, in presenting data from Unit III, we use the composite depths of Sites 885 and 886 suggested by Dickens et al. (this volume). These composite depths are denoted by "mcd" (meters composite depth) rather than "mbsf" (meters below seafloor), and have two implications pertinent to this study. First, a core break occurs at 63.8 mbsf in Hole 886C. We assume a recovery gap of 0.75 m spans this break (Dickens and Owen, 1993); upcore profiles presented here, therefore, lack data between 61.20 and 61.95 mcd. Second, three prominent hiatuses exist within Unit III sediment at Hole 885A. These occur between 48.65–48.70 mbsf, 49.41–49.55 mbsf, and 50.40–50.65 mbsf (Dickens et al., this volume); thus, the sedimentary record in the lowermost sediment at Hole 885A is discontinuous.

## ANALYTICAL PROCEDURES

All bulk samples were initially freeze-dried, gently homogenized within a ceramic mortar and pestle, and split into two replicate sets: one for mineralogical and electron microscopic analyses, the other for bulk chemical analyses. Five samples from the first set of replicates (Sample 145-886B-7H-6, 80 cm, and Samples 145-886C-7H-6, 80 cm, -8H-1, 80 cm, -8H-3, 80 cm, and -8H-6, 80 cm) were analyzed for qualitative bulk mineralogical composition by X-ray diffraction (XRD) on a Phillips 3100 X-ray generator. Instrumental conditions were as follows: CuK $\alpha$  radiation with a graphite monochromator, 35 KV, 15 mA, goniometer scan from 4° to 42° 2 $\theta$ , step size of 0.01, and count time of 1 s. Individual samples for these XRD analyses were reground within an agate mortar and pestle and adhered to glass slides with acetone. Portions of these same five samples (and a split of Sample 145-886B-7H-2, 80 cm) also were placed under a Hitachi S-570 scanning electron microscope (SEM) equipped with a back-scattered electron (BSE) imaging and Kevex energy dispersive spectroscopy (EDS) system. The purpose of this work was to determine morphology and semiquantitative elemental compositions (by EDS) of individual sedimentary phases (particularly amorphous oxyhydroxides). Individual samples were sprinkled in situ with acetone onto carbon wafers and subsequently coated with carbon. Analyses by EDS were conducted with samples at a working distance of 23 mm, a 15° tilt to the beam, and 20 KV.

We analyzed 69 samples from the second set of replicates for bulk elemental chemistry by instrumental neutron activation analysis (INAA) using the nuclear reactor and counting facilities at the Phoenix Memorial Laboratory, University of Michigan. These samples were reground and homogenized within a ceramic mortar and pestle. Approximately 250 mg were then enclosed within prewashed, high-purity quartz tubes, irradiated for 20 hr on a rotating holder, counted for 67 min after a decay of 1 week, and analyzed for As, La, Lu, Mo, Sm, and Yb. These same samples were recounted for 67 min after a decay of 5 weeks, and analyzed for Ce, Co, Cr, Cs, Eu, Fe, Hf, Sb, Sc, Tb, Th, and Zn. Samples received a thermal neutron flux of approximately  $5 \cdot 10^{12}$  neutrons/cm<sup>2</sup>/s and were counted using a pair of multiplexed Ge-Li gamma detectors. Concentrations for all elements were obtained through standard comparison with NBS-SRM-1633a (coal fly ash). Half-lives and gamma lines used for these analyses (Table 1) were taken from Browne and Firestone (1986).

In general, analytical precision ( $1\sigma$ ) was within less than 5% for analyses of As, Ce, Co, Cs, Eu, Fe, Hf, La, Sb, Sc, Sm, Th, and Yb, and between 5% and 10% for Cr, Lu, Mo, Tb, and Zn. Including other random errors (e.g., geometrical differences between samples during

irradiation and counting, slight changes in neutron flux during irradiation), we estimate total errors ( $1\sigma$ ) in reported concentrations to be between 3% and 8% for the first suite of elements, and less than 7% to 13% for the second suite of elements. We also analyzed 15 "Leg 92 Standard Sediment" (Owen and Ruhlin, 1986), 7 NBS-SRM-679 (brick clay), and 3 NBS-SRM-688 (basalt rock) standards in the same batches as samples from Sites 885 and 886 to evaluate INAA precision and accuracy. Results from these standard analyses along with reported standard concentrations are shown in Table 2. The standard deviation for these repeated analyses (except Zn) typically are within the ranges determined from individual analyses of samples from Sites 885 and 886. Published elemental concentrations for the three standards generally are within the standard deviation of measured values. Exceptions include As, Eu, La, Sc, Sm, and Tb for Leg 92 Standard Sediment, Sc for NBS-SRM-679, and Co, Lu, Sc, and Yb for NBS-SRM-688. These discrepancies suggest that, even though precision is high for these elements, our reported concentrations may have a consistent analytical offset.

The Ce anomaly (Ce/Ce\*) is a measure of how enriched or depleted Ce is relative to adjacent REE elements in a given sample compared with concentrations of the same REEs in a given standard (e.g., De Baar et al., 1988). For this study, Ce/Ce\* is defined as follows (e.g., Toyoda et al., 1990):

$$\text{Ce/Ce}^* = \left( \frac{5 \cdot \text{Ce/Ce}_{\text{NASC}}}{(4 \cdot \text{La/La}_{\text{NASC}}) + \text{Sm/Sm}_{\text{NASC}}} \right),$$

where NASC represents North American Shale Composite (Ce = 83 ppm, La = 41 ppm, and Sm = 7.5 ppm; Piper, 1974). The choice of using Sm rather than Pr or Nd (cf. De Baar et al., 1988; Toyoda et al., 1990; Murray et al., 1991) arises because of large analytical errors associated with obtaining Nd concentrations by INAA, and yet still conveys the concept of normalizing Ce to surrounding REEs.

## RESULTS AND DISCUSSION

### Hypothesized Hydrothermal Sequence

If the proposed origin for the Chinook Trough is correct, then sediment deposited immediately south of the eastern end of the Chinook Trough should exhibit at least three characteristics. First, sediment deposited between approximately 65 and 75 Ma should be significantly enriched in distal hydrothermal sediment. This age marks a time when the Kula-Pacific Ridge probably lacked an axial valley, and also was within several hundred kilometers of Sites 885 and 886. Lyle et al. (1986) have shown that an obvious hydrothermal signal can be found in sediment upward of 600 km from the East Pacific Rise. Using the aforementioned spreading rates of Mammerickx and Sharman (1988)—a rifting age of 80 Ma, and an initial distance of 60 km between Sites 885 and 886 and the Kula-Pacific Ridge—the distance between Sites 885 and 886 and the Kula-Pacific Ridge would be approximately 590 km at 65 Ma. Sediment deposited before 75 Ma also should contain distal hydrothermal precipitates; however, the abundance of this component might be strongly regulated by the efficiency of the inferred axial valley to serve as a trap for buoyant plumes.

Second, the accumulation rate of distal hydrothermal components should decrease in a roughly exponential pattern from approximately 75 Ma onward (assuming near constant bottom-water flow and particle injection rates) because the Kula-Pacific spreading center moved northward relative to the trough (Fig. 3) and Sites 885 and 886. An increase in the accumulation of hydrothermal components (i.e., a "spike") also might be expected at or near 75 Ma. Not only would this be the time at which buoyant plumes could escape entrapment, but it also may mark a time of tectonic reorganization (as evident by the stepwise change in spreading rate).

Third, bulk sediment should lack carbonate because tectonic models concerning the evolution of the Chinook Trough (e.g., Woods and Davies, 1982; Rea and Dixon, 1983; Mammerickx and Sharman,

**Table 1. Parameters used for INAA analyses of samples in this study.**

Element	Gamma energy (KeV)	Half-life
As	559.08	1.097 (d)
Ce	145.44	32.50 (d)
Co	1332.50	5.271 (y)
Cr	320.08	27.704 (d)
Cs	795.87	2.062 (y)
Eu	1408.00	13.33 (d)
Fe	1099.25	44.496 (d)
Hf	482.00	42.39 (d)
La	487.03	1.678 (d)
Lu	208.36	6.71 (d)
Mo	140.47	2.747 (d)
Sb	564.37	2.70 (d)
Sc	889.25	83.83 (d)
Sm	103.18	1.946 (d)
Tb	879.37	72.30 (d)
Th	312.01	27.00 (d)
Yb	396.33	4.19 (d)
Zn	1115.52	244.10 (d)

Notes: Parameter data from Browne and Firestone (1986). (d) = days, and (y) = years.

1988; Atwater et al., 1993) imply that Late Cretaceous paleodepths for locations immediately south of the eastern end of the trough were below the calcite compensation depth (CCD; Fig. 4). The basement beneath Sites 885 and 886 (not recovered, Rea, Basov, Janecek, Palmer-Julson, et al., 1993) is thought to have formed at the now inactive Emperor Trough spreading center during the Neocomian at approximately 125 Ma (Rea and Dixon, 1983; Renkin and Sclater, 1988). Using a minimum depth for the Emperor Trough spreading center of 2.75 km and crustal subsidence curves (e.g., Rea and Leinen, 1986), Sites 885 and 886 were at a minimum paleodepth of 4.4 km at 80 Ma. Such a paleodepth is below estimated Late Cretaceous CCD curves (3–4 km; Van Andel, 1975; Boss and Wilkinson, 1991), even when an equatorial Cretaceous position for these sites is considered.

Shipboard observations (smear-slide analyses and coulometry) have demonstrated that Unit III sediment at Sites 885 and 886 is devoid of carbonate (Rea, Basov, Janecek, Palmer-Julson, et al., 1993). The following discussion examines whether the other expectations concerning the origin of the Chinook Trough are evident in sediment deposited at Sites 885 and 886.

### Lowermost Unit III Sediment

Sample 145-885A-6H-7, 5 cm, and Samples 145-886C-8H-6, 5 cm, -8H-6, 30 cm, and -8H-6, 80 cm, are from the lowermost very dark brown portion of Unit III (>69.5 mcd), and were deposited within 1.4 m of Unit IV basalt (Dickens et al., this volume). Mineralogical and chemical analyses indicate that these samples are significantly enriched in distal hydrothermal components. Indeed, because this interval of the sedimentary column lacks biogenic and/or detrital diluents, these samples reflect a near-pure distal hydrothermal end-member.

The bulk mineralogy of Sample 145-886C-8H-6, 80 cm, consists of moderately well-crystallized goethite, apatite, and hematite; typical detrital minerals (quartz, feldspar, and clays) are noticeably absent (Fig. 5). The primary mineralogy of goethite and apatite is essentially that of other distal hydrothermal sequences, and the bulk XRD pattern for Sample 145-886C-8H-6, 80 cm (excluding hematite) displays remarkable resemblance to those of carbonate-free Quaternary and Neogene distal hydrothermal sediment recovered on Deep Sea Drilling Project (DSDP) Leg 92 (Barrett et al., 1986). Although hematite was not found in DSDP Leg 92 sediment (Barrett et al., 1986), it has been reported in other distal hydrothermal sequences (e.g., Meylan et al., 1981). The bulk XRD pattern of Sample 145-886C-8H-6, 80 cm, does not show a peak for nontronite. However, bulk nontronite concentrations may exceed 20% in lowermost samples of Sites 885 and 886 (E. Arnold, pers. comm., 1994). The presence of nontronite again is consistent with a predominantly hydrothermal origin for lowermost samples of Sites 885 and 886 inasmuch as nontronite in pelagic

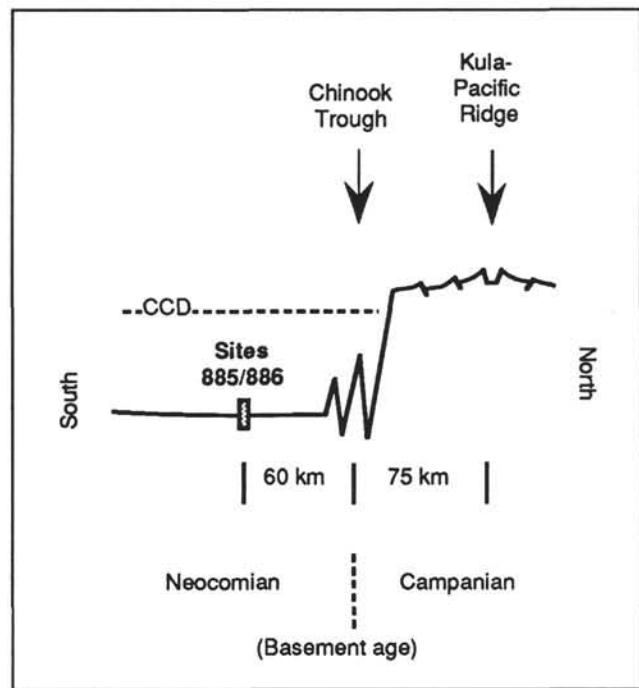


Figure 4. Reconstruction of depositional environment at Sites 885 and 886 at 76 Ma using a rifting age of 80 Ma and a maximum constant spreading rate of 1.8 cm/yr following initial rifting. Sites 885 and 886 would be approximately 135 km from the Kula-Pacific Spreading Ridge. Note that basement ages are markedly different across the Chinook Trough, and a potential distal hydrothermal signal would be deposited below the CCD.

environments is often associated with hydrothermal deposition (e.g., Meylan et al., 1981; Honnorez, Von Herzen, et al., 1983).

Electron microscopic analyses provide further detail concerning the mineralogical composition. Phases found in Sample 145-886C-8H-6, 80 cm, using SEM/BSE/EDS include abundant Fe-Mn oxyhydroxides, lesser amounts of Ca-phosphates, small quantities of aluminosilicates, and individual euhedral crystals of barite. Barrett et al. (1988) have estimated that Quaternary and Neogene distal hydrothermal sediment consists of approximately 30%–50% (by volume) amorphous Fe-Mn oxyhydroxides. Visual inspection (using the SEM) suggests that Fe-Mn oxyhydroxides with no apparent crystal habit comprise at least 30% of Sample 145-886C-8H-6, 80 cm. Apatite, including apatite concretions (Plate 1), accounts for upward of several percent (by volume) of Sample 145-886C-8H-6, 80 cm. This apatite may be of biogenic origin, but more likely reflects postburial remobilization of  $\text{PO}_4^{3-}$ , which previously was scavenged by hydrothermally derived Fe oxyhydroxides (cf. Feely et al., 1990b). The barite crystals also may be of biogenic and/or hydrothermal origin (Dehairs et al., 1980; Feely et al., 1990a). Sulfide phases (e.g., sphalerite) were not found in this sample. This latter observation is consistent with a distal hydrothermal origin inasmuch as hydrothermally derived sulfides typically are deposited within 1 km of venting regions (e.g., Feely et al., 1990a).

Lowermost samples from Holes 885A and 886C also are chemically similar to Holocene and Neogene distal hydrothermal sediment deposited along the flanks of the East Pacific Rise (Table 3). Concentrations of Fe (except Sample 145-886C-8H-6, 80 cm) are within the range (25%–39%) typical of more recently deposited distal hydrothermal sediment (Barrett et al., 1988) and are consistent with mineralogical analyses indicating that the lowermost sediment of Holes 885A and 886C is primarily composed of Fe-Mn oxyhydroxides. Sample 145-886C-8H-6, 80 cm, may contain enough apatite and/or nontronite such that bulk Fe in this sample is diluted to below 25%.

**Table 2. Comparison of INAA results for Leg 92 Standard Sediment, NBS-SRM-679 (brick clay), and NBS-SRM-688 (basalt rock) standards to values published in literature.**

Element	Measured (N = 15)	Leg 92 S.S. SD	Published <sup>1</sup>	Measured (N = 7)	NBS-SRM-679 SD	Published <sup>2</sup>	Measured (N = 3)	NBS-SRM-688 SD	Published <sup>3</sup>
As	57.8	0.84	49	9.7	0.97	NR	2.5	0.16	2.5
Ce	10	1.1	9.32	106	2.6	105	12	2.7	13
Co	20	1.2	20	26	1.4	26	45	1.9	49
Cr	<4.1		2.30	109	4.3	109.7	310	16	310
Cs	<0.5		NR	9.9	0.28	9.6	<0.7		0.24
Eu	1.19	0.11	1.35	1.84	0.12	1.9	0.99	0.16	1.01
Fe	6.2	0.15	6.12	9.1	0.14	9.05	6.9	0.32	7.17
Hf	<0.4		0.30	4.7	0.43	4.6	1.6	0.21	1.55
La	29.2	0.92	25.7	53.0	0.55	NR	5.0	0.31	5.3
Lu	0.42	0.06	0.46	0.52	0.05	NR	0.27	0.02	0.35
Mo	31	3.9	NR	<5		NR	<4		NR
Sb	2.28	0.16	2.31	0.87	0.19	NR	<3.5		0.3
Sc	1.70	0.09	1.89	23.1	0.46	22.5	36.0	0.69	38
Sm	4.40	0.13	5.26	9.17	0.14	NR	2.3	0.30	2.5
Tb	0.84	0.10	0.68	1.2	0.14	NR	? 0.4		0.52
Th	<0.4		NR	13.9	0.36	14	<0.5		0.36
Yb	3.0	0.24	2.73	3.6	0.3	NR	1.9	0.09	2.05
Zn	110	24	142	130	22	150	70	20	84

Notes: N = number of analyses, S.S. = Standard Sediment, SD = standard deviation, and NR = value not reported. Sources for published data are as follows: 1 = mean values reported in Owen and Ruhlin (1986); 2 = National Bureau of Standards Certificate of Analyses; and 3 = mean consensus values reported in Gladney et al. (1987). All elements reported in ppm, except for Fe (in percent).

**Table 3. Elemental comparison between lowermost sediment at Holes 885A and 886C and Pleistocene distal hydrothermal sediment deposited on the flank of the East Pacific Rise.**

Element	CaCO <sub>3</sub> -free Leg 92 S.S.	886C-8H-6, 5 cm	886C-8H-6, 30 cm	886C-8H-6, 80 cm	885A-6H-7, 5 cm
As	292	385	359	281	352
Ce	51	23	35	32	59
Co	101	94	86	69	77
Cr	<21	<12	15	12	18
Cs	<2.6	<1.1	<1.1	<1.1	1.2
Eu	6.0	8.3	8.8	11.5	10.8
Fe	31.3	32.3	30.3	23.7	26.0
Hf	<2.1	2.5	1.6	1.7	2.8
La	147	185	174	293	240
Lu	2.1	1.8	1.9	4.5	2.2
Mo	160	560	379	280	180
Sb	11.5	22.7	21.8	17.4	28.8
Sc	8.6	9.5	11.6	18.3	14.2
Sm	22.2	33.9	36.1	43.4	45.8
Tb	4.0	4.7	5.3	7.3	6.7
Th	1.5	<0.9	0.7	<0.7	2.0
Yb	15.2	13.6	12.5	28.5	18.1
Zn	556	700	700	390	660
Ce/Ce*	0.18	0.06	0.10	0.06	0.12

Notes: Concentrations of Leg 92 Standard Sediment (S.S.) reported in this table are from this study (Table 2) rather than those reported in Ruhlin and Owen (1986) to eliminate potential analytical biases (i.e., for As, Eu, La, Sc, Sm, and Tb). These concentrations were converted to carbonate-free values (CaCO<sub>3</sub> = 80.2%) to eliminate biogenic dilution. Ce/Ce\* values from definition for cerium anomaly provided in text. All elements reported in ppm, except for Fe (in percent).

The trace metals As, Mo, Sb, and Zn are present in concentrations 1–2 orders of magnitude higher than in Late Cretaceous Pacific red clay deposited approximately 600 km away at Site LL44-GPC3 (Kyte et al., 1993). The pronounced negative Ce anomalies (Ce/Ce\* < 0.12) further support a hydrothermal origin for lowermost Unit III samples; such Ce/Ce\* values in bulk pelagic sediment typically are found only in sediment dominated by hydrothermal oxyhydroxides (e.g., Ruhlin and Owen, 1986; Murray et al., 1991).

The deficiency of certain elements within lowermost samples from Holes 885A and 886C also is consistent with an interpretation that this sediment is almost exclusively of hydrothermal origin. Barrett et al. (1988) have noted that distal hydrothermal sediment is significantly depleted in Co (<250 ppm) relative to other ferromanganese deposits. Cobalt concentrations in the lowermost sediment

samples are lower than 94 ppm. Elements commonly associated with detrital phases (i.e., Cr, Cs, Hf, Sc, and Th) are depleted relative to Late Cretaceous red clay deposited at LL44-GPC3 (Kyte et al., 1993). This latter observation is consistent with the mineralogical results, inasmuch as silicate phases (e.g. quartz, feldspars, and clays) were not detected in the bulk XRD pattern of Sample 145-886C-8H-6, 80 cm.

### Compositional Variations Within Unit III Sediment

Sediment of the lower portion of Unit III (>56 mcd) consists of two primary components: hydrothermal and terrigenous. The relative proportion of hydrothermal to terrigenous components progressively decreases upcore such that sediment below 66 mcd is composed almost exclusively of the hydrothermal component (as discussed in the previous section), and sediment above 59 mcd is composed predominantly of the terrigenous component.

Results from bulk XRD analyses (Fig. 5) show a pronounced upcore mineralogical change. The detected bulk mineralogy of Sample 145-886C-8H-3, 80 cm (4.75 m above Unit IV basalt) is somewhat similar to that of Sample 886C-8H-6, 80 cm, and consists of moderately well-crystallized goethite and apatite. Quartz is present, but peaks for feldspar and clay minerals again are noticeably absent. Further upcore (Sample 886C-8H-1, 80 cm; 7.75 m above Unit IV basalt), quartz, feldspar, smectite, illite, and goethite each were detected, but peaks for goethite are relatively small compared to those of quartz. Apatite was not detected in Sample 145-886C-8H-1, 80 cm. The detected bulk mineralogy of Samples 145-886C-7H-6, 80 cm, and 145-886B-7H-6, 80 cm (>10 m above Unit IV basalt) consists of quartz, smectite, illite, kaolinite, and feldspar. Thus, the minerals detected in the bulk sediment can be conveniently grouped as either oxyhydroxide/phosphates or silicates, and the relative proportion of oxyhydroxide/phosphates to silicates decreases upcore.

The upcore variation from oxyhydroxide/phosphates (hydrothermal) to silicates (terrigenous) also is apparent using SEM/BSE/EDS. Sample 145-886C-8H-3, 80 cm, contains predominantly Fe-Mn oxyhydroxide phases, with minor amounts of Ca-phosphates (apatite), "web-like" aluminosilicate phases (clays), and abiogenic silica (quartz); clays appear to be significantly more abundant than quartz and/or apatite. Dispersed Mn micronodules also are observed in this sample (in contrast to Sample 145-886C-8H-6, 80 cm). Layers of small (<1 cm in diameter) ferromanganese nodules also were described in the core barrel sheets for Core 145-886C-7H (Rea, Basov, Janecek, Palmer-Julson, et al., 1993). At present, it is unclear why these nodules formed and why they only exist in certain samples.

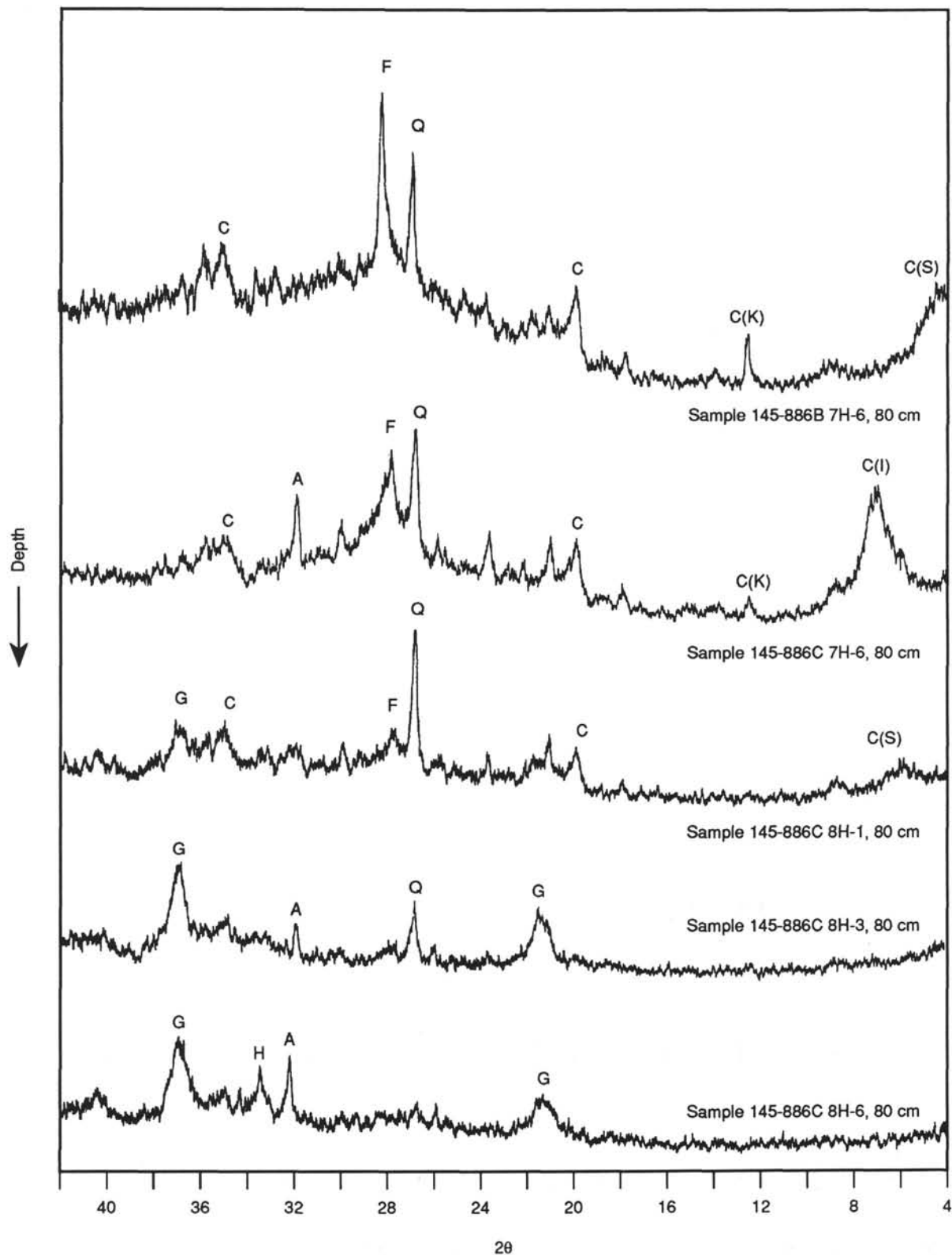


Figure 5. Bulk XRD patterns for sediment from Unit III of Site 886 displayed in order of descending composite depth for Sites 885 and 886. Note that the detected bulk mineralogy of Sample 145-886C-8H-6, 80 cm, consists of goethite (G), apatite (A), and hematite (H), but these minerals are replaced by quartz (Q), feldspar (F), and clays (C; K = kaolinite, S = smectite, and I = illite) with increasing distance upcore. Not apparent on these plots are abundant amorphous Fe-Mn oxyhydroxides and nontronite in the lowermost sediment of Unit III.

Table 4. Bulk chemistry of sediment samples from Holes 885A, 886B, and 886C.

Core, section, interval (cm)	Depth (mbsf)	Composite depth (m)	As	Ce	Co	Cr	Cs	Eu	Fe	Hf	La	Lu	Mo	Sb	Sc	Sm	Tb	Th	Yb	Zn	Ce/Ce*
145-885A-																					
6H-2, 5-10	44.15	52.07	7.3	126.6	55.2	62.8	12.2	2.43	3.89	3.97	44.6	0.50	***	2.08	31.83	10.73	1.48	14.4	4.09	125	1.32
6H-2, 80-85	44.90	52.91	8.6	142.8	79.1	73.4	13.2	2.08	4.42	4.92	41.9	0.42	***	2.50	38.32	9.77	1.50	17.8	3.66	222	1.60
6H-3, 5-10	45.65	53.55	***	164.7	89.3	66.5	13.7	2.55	4.54	5.34	48.4	0.42	***	2.29	42.79	11.14	1.21	17.7	3.94	189	1.60
6H-3, 80-85	46.40	54.20	8.2	177.4	128.7	79.4	12.3	3.23	4.46	5.52	53.9	0.88	6.8	2.52	42.18	14.37	1.72	18.9	5.86	207	1.49
6H-4, 5-10	47.15	54.84	9.1	179.3	155.1	65.8	13.3	3.22	4.79	6.26	53.2	0.74	5.4	2.77	46.60	14.33	1.93	17.0	4.65	160	1.52
6H-4, 80-85	47.90	55.46	6.3	235.1	196.5	57.1	10.4	6.29	4.57	5.72	84.8	1.62	14.0	2.58	36.35	25.84	4.47	23.6	11.21	210	1.21
6H-5, 5-10	48.65	56.15	31.3	259.5	259.1	41.7	7.0	12.83	6.09	6.86	168.2	3.13	25.7	5.14	36.84	51.86	7.66	19.5	23.03	210	0.67
6H-5, 30-35	48.90	59.04	15.9	205.7	153.9	36.3	6.4	8.53	5.56	4.97	114.8	1.95	17.6	3.28	30.78	33.82	5.07	10.1	14.32	162	0.79
6H-5, 81-86	49.41	60.26	43.9	198.2	142.3	49.5	4.8	16.76	7.71	5.03	233.9	3.53	26.2	5.35	41.82	65.76	11.83	7.8	26.94	194	0.38
6H-5, 105-110	49.65	62.40	65.6	173.3	127.9	48.7	4.5	18.02	8.43	5.40	260.3	3.74	26.1	6.43	42.12	72.71	10.75	8.7	27.39	281	0.30
6H-6, 5-10	50.15	62.90	136.3	230.8	118.4	47.7	5.0	20.15	11.42	6.20	320.6	4.79	43.8	11.51	42.68	85.43	13.47	12.7	34.78	425	0.33
6H-6, 30-35	50.40	63.25	231.5	191.5	117.5	32.7	5.1	16.00	16.92	6.33	240.7	2.72	69.4	19.60	29.80	64.42	9.93	8.7	21.59	431	0.36
6H-6, 80-85	50.90	69.57	347.3	72.7	113.9	22.8	1.1	13.17	27.41	2.83	244.6	2.61	158.8	30.16	17.63	52.80	8.49	***	18.90	674	0.14
6H-6, 105-110	51.15	69.79	354.2	54.8	78.9	19.3	1.7	11.85	25.60	3.12	260.3	2.37	165.8	29.90	14.30	48.63	7.11	1.6	17.99	624	0.10
6H-7, 5-10	51.53	70.13	352.3	58.7	77.4	18.0	1.2	10.84	26.02	2.75	239.6	2.24	178.5	28.78	14.18	45.83	6.68	2.0	18.12	661	0.12
6H-7, 30-35	51.78	70.38	370.5	43.9	84.6	14.6	1.2	11.36	26.93	2.54	271.7	2.51	166.9	31.18	12.34	46.50	7.16	***	18.88	704	0.08
145-886B-																					
7H-2, 5-10	50.85	52.60	8.2	130.7	69.1	61.7	11.3	1.99	4.49	5.23	40.6	0.49	***	2.22	31.96	8.76	0.74	15.5	3.14	181	1.54
7H-2, 80-85	51.60	53.35	***	145.9	104.1	63.8	14.1	2.17	4.50	5.25	42.2	0.47	5.9	2.06	40.64	9.32	0.94	16.2	3.01	182	1.64
7H-3, 5-10	52.35	54.10	7.6	158.8	113.1	58.7	10.3	3.87	4.01	5.75	52.2	0.94	4.0	2.89	37.27	16.29	2.41	16.2	5.69	120	1.32
7H-3, 80-85	53.10	54.85	10.5	176.2	152.1	58.1	12.6	3.07	4.82	6.30	49.7	0.61	12.6	2.41	46.29	13.38	2.17	17.2	4.86	185	1.60
7H-3, 105-110	53.35	55.10	8.9	180.1	157.7	64.7	11.0	3.97	4.16	5.80	52.1	0.84	6.6	2.49	42.14	16.94	1.99	16.5	5.65	229	1.48
7H-3, 130-135	53.60	55.35	10.5	185.9	157.9	50.6	8.8	5.30	4.11	5.58	64.0	1.37	17.0	2.74	34.99	23.00	2.99	17.4	9.37	166	1.20
7H-4, 5-10	53.85	55.42	12.1	248.6	221.2	44.8	10.8	7.15	4.50	6.48	91.8	1.73	17.6	2.78	35.61	29.71	3.83	23.0	12.60	197	1.16
7H-4, 80-85	54.60	55.78	44.2	267.1	272.0	48.7	6.3	12.76	6.20	5.96	184.5	3.02	37.8	4.98	37.07	54.50	7.24	17.0	23.59	161	0.64
7H-5, 5-10	55.35	56.69	16.4	268.0	261.7	43.5	7.1	5.97	4.53	5.84	92.9	1.60	38.6	2.87	31.03	24.40	4.43	16.3	11.04	127	1.31
7H-5, 80-85	56.10	57.60	13.7	270.7	209.4	61.6	11.2	5.80	4.73	6.45	83.4	1.32	24.2	2.89	36.02	24.39	3.60	17.4	9.70	180	1.43
7H-6, 5-10	56.85	58.42	13.8	262.9	189.2	43.4	7.9	6.24	4.91	5.71	91.2	1.59	33.2	2.41	32.68	26.77	4.33	11.0	10.74	117	1.27
7H-6, 80-85	57.60	59.08	13.6	233.3	169.9	22.0	5.4	5.88	5.03	5.91	73.0	1.48	35.1	2.16	30.59	23.45	4.35	9.6	10.90	103	1.37
7H-7, 5-10	58.35	59.80	14.9	251.0	177.4	55.4	8.1	9.44	5.63	5.99	129.3	2.14	26.9	3.13	33.10	38.22	6.73	11.2	15.73	240	0.85
7H-CC, 5-10	59.04	60.49	16.6	210.2	159.0	38.9	5.6	10.38	6.42	4.71	144.0	2.48	32.5	3.25	38.08	41.34	7.21	8.2	16.87	275	0.65
145-886C-																					
7H-1, 5-10	54.35	52.87	***	113.7	65.4	59.8	10.8	2.16	3.82	4.18	37.9	0.43	***	1.69	31.66	9.05	1.68	14.5	3.38	147	1.40
7H-2, 5-10	55.85	53.90	9.8	171.3	129.4	69.4	12.5	3.63	4.33	5.76	54.6	0.86	13.6	2.38	39.54	15.11	1.89	17.3	5.67	203	1.41
7H-2, 80-85	56.60	54.42	11.6	178.4	155.5	69.5	13.7	2.98	4.61	5.93	50.0	0.93	13.6	2.17	45.00	13.62	1.57	16.5	5.21	125	1.61
7H-3, 5-10	57.35	54.94	9.6	181.9	136.9	67.3	12.7	3.18	4.64	6.60	49.2	0.69	13.1	2.14	42.03	14.02	2.04	16.3	4.82	153	1.64
7H-3, 80-85	58.10	55.50	12.1	245.3	220.8	54.5	10.4	6.82	4.62	6.24	87.3	2.19	18.7	3.04	36.85	28.69	4.60	23.9	11.86	112	1.20
7H-4, 5-10	58.85	56.25	17.8	250.9	274.0	41.3	7.1	6.25	4.71	6.07	101.5	1.95	41.4	3.11	29.89	25.56	4.45	17.3	13.10	122	1.14
7H-4, 80-85	59.60	57.00	13.0	283.3	225.2	56.3	10.1	6.06	4.57	5.89	82.1	1.58	32.9	2.52	36.82	24.49	3.78	17.5	10.48	150	1.51
7H-5, 5-10	60.35	57.75	13.1	295.6	215.0	43.4	9.0	5.69	4.65	6.64	78.6	1.26	38.6	2.61	33.40	24.02	3.20	16.2	8.60	145	1.64
7H-5, 80-85	61.10	58.50	14.3	257.3	185.4	38.4	9.2	6.29	4.87	5.73	85.2	1.64	26.0	2.56	33.57	25.07	4.38	10.7	10.61	139	1.33
7H-6, 5-10	61.85	59.25	12.0	197.4	132.1	36.4	6.4	7.05	5.52	5.21	89.8	1.64	30.3	2.60	30.36	27.85	4.61	8.7	11.35	149	0.95
7H-6, 30-35	62.10	59.50	19.0	266.2	191.2	52.4	6.2	10.18	5.38	4.93	137.2	2.58	33.1	2.79	34.17	40.24	7.03	12.3	17.80	155	0.86
7H-6, 80-85	62.60	60.00	19.5	187.7	169.0	42.1	4.8	10.03	6.40	5.08	130.7	2.74	28.6	2.39	37.38	36.56	6.73	7.3	16.64	145	0.64
7H-6, 105-110	62.85	60.25	17.0	183.3	164.0	38.7	5.1	12.07	5.96	4.86	158.1	2.64	28.4	2.64	36.78	46.69	8.81	9.0	19.77	230	0.51
7H-7, 5-10	63.35	60.75	15.2	153.8	116.9	52.3	9.3	7.68	4.92	4.50	112.9	1.73	58.2	2.88	29.14	31.75	4.72	12.0	12.43	315	0.61
7H-7, 30-35	63.60	61.00	17.4	162.1	106.3	64.0	10.2	8.45	5.12	5.07	117.7	1.93	38.7	1.93	32.40	33.00	5.85	12.2	13.35	177	0.61
8H-1, 5-10	63.85	62.00	80.4	200.3	121.2	44.9	5.8	16.03	8.98	5.01	248.3	3.67	101.5	7.12	40.26	66.08	9.73	10.9	26.93	305	0.37
8H-1, 30-35	64.10	62.25	117.4	267.3	142.7	58.5	5.1	18.90	11.48	6.41	283.7	4.51	85.0	9.65	43.23	76.22	12.48	11.4	30.84	383	0.43
8H-1, 80-85	64.60	62.75	120.4	244.9	127.2	47.4	5.6	14.31	11.56	6.74	212.4	3.62	86.2	9.54	38.82	55.88	9.92	12.9	22.80	323	0.52
8H-1, 105-110	64.85	63.00	135.8	247.9	118.6	48.8	5.8	15.74	12.49	5.72	234.2	3.75	79.8	10.26	38.14	63.85	10.57	12.9	26.29	425	0.48
8H-2, 5-10	65.35	63.50	148.7	231.3	163.8	38.3	6.2	13.53	13.86	7.59	193.0	2.48	124.6	11.48	32.02	53.92	7.47	11.6	18.33	254	0.54
8H-2, 30-35	65.60	63.75	166.9	237.8	162.6	46.9	4.9	12.57	14.44	6.06	199.9	2.68	107.7	12.90	31.15	54.19	7.74	10.2	19.22	345	0.54
8H-2, 80-85	66.10	64.25	187.8	233.0	170.9	42.8	6.0	13.28	16.50	6.96	197.1	2.89	100.5	14.81	31.11	51.74	8.11	10.2	17.29	369	0.54
8H-2, 105-110	66.35	64.50	211.6	229.2	146.0	38.9	5.9	14.78	18.46	7.33	225.9	3.14	122.9	16.27	31.64	60.52	9.04	9.0	22.67	420	0.46
8H-3, 5-10	66.85	65.00	252.3	196.9	131.1	38.2	4.7	16.47	20.13	7.06	251.8	3.17	160.5	18.04	30.11	67.89	10.08	8.8	23.76	476	0.35
8H-3, 30-35	67.10	65.25	252.5	193.6	132.9	39.4	3.7	17.82	21.78	6.51	276.8	3.82	122.0	18.17	30.77	71.67	10.86	8.3	25.67	517	0.32
8H-3, 80-85	67.60	65.75	341.8	151.0	101.2	28.6	2.8	18.58	28.39	6.76	272.9	4.00	172.9								

Table 4 (continued).

Core, section, interval (cm)	Depth (mbsf)	Composite depth (m)	As	Ce	Co	Cr	Cs	Eu	Fe	Hf	La	Lu	Mo	Sb	Sc	Sm	Tb	Th	Yb	Zn	Ce/Ce*
8H-4, 105-110	69.35	67.50	275.8	89.6	80.0	42.6	1.6	30.01	27.70	3.49	482.4	4.98	237.3	19.42	24.44	121.69	17.83	2.7	37.27	650	0.09
8H-5, 5-10	69.85	68.00	293.4	92.2	85.2	14.9	2.4	18.43	27.45	3.65	358.8	3.23	367.9	21.15	20.56	78.75	9.92	3.3	26.43	621	0.12
8H-5, 30-35	70.10	68.25	293.9	82.5	89.0	26.5	1.7	16.81	27.48	3.06	341.0	3.08	306.0	20.10	19.36	70.78	10.05	2.2	23.47	560	0.12
8H-5, 80-85	70.60	68.75	263.7	90.6	86.1	22.3	3.5	20.01	25.76	3.33	360.4	3.94	233.9	19.57	20.98	80.04	11.91	2.9	24.63	425	0.12
8H-5, 105-110	70.85	69.00	266.4	86.3	79.0	35.9	1.7	20.30	25.98	3.46	363.8	3.57	243.4	17.79	21.30	84.78	11.67	2.3	26.66	601	0.11
8H-6, 5-10	71.35	69.50	385.1	23.1	93.8	***	***	8.35	32.25	2.47	184.6	1.79	563.2	22.69	9.49	33.86	4.71	***	13.57	702	0.06
8H-6, 30-35	71.60	69.75	359.5	35.0	86.4	14.7	***	8.77	30.33	1.58	173.8	1.88	379.0	21.91	11.56	36.09	5.31	0.7	12.47	700	0.10
8H-6, 80-85	72.10	70.25	281.1	32.0	68.6	11.9	***	11.50	23.75	1.74	293.4	4.49	282.5	17.42	18.32	43.39	7.32	***	28.49	396	0.06

Notes: All elements reported in ppm, except Fe (in percent). All values have not been rounded to reflect significant figures. Triple asterisks (\*\*\*) = concentrations below detection limit. Cerium anomaly (Ce/Ce\*) calculated according to text.

Sample 145-886C-8H-1, 80 cm, is compositionally similar to Sample 145-886C-8H-3, 80 cm, although it contains greater proportions of clay and quartz. Apparent grains of feldspar also can be found in this sample. Samples 145-886C-7H-6, 80 cm, and 145-886B-7H-6, 80 cm, consist mostly of clays, quartz, and feldspar. Euhedral, prism-shaped Ca-Fe aluminosilicates of unknown mineralogy also are present in this sample. Sample 145-886B-7H-2, 80 cm, (not examined by XRD), is somewhat different than Samples 145-886C-7H-6, 80 cm, and 145-886B-7H-6, 80 cm, in that it contains obvious biogenic silica and abundant euhedral barite.

The high-resolution bulk chemistry results (Table 4) also suggest an upcore transition from predominantly hydrothermal to terrigenous deposition. The five elements that characterize distal hydrothermal sediment (As, Fe, Mo, Sb, and Zn) are greatly enriched in the lowermost sediment of Holes 885A and 886C (>66 mcd), but decrease in concentration upcore. Bulk Fe concentrations decrease from 25%–30% to 4.5%–5% between 66 and 59 mcd (Fig. 6). Iron concentrations of 4.5%–5% likely represent “background” values (e.g., lattice-bound Fe within clays) because such concentrations also are determined for more recent (Pliocene-Pleistocene), biogenic-free sediment at Sites 885 and 886 (Dickens et al., this volume). The concentration profiles of As, Sb, and Zn are highly correlated with that of Fe ( $r > 0.94$ ). This relationship implies that these elements are not scavenged from seawater; elements that are scavenged by hydrothermally derived oxyhydroxides (e.g., REEs) exhibit a progressive upcore increase in their element/Fe ratio (cf. Ruhlin and Owen, 1986; German et al., 1990). The correlation between Fe and Mo ( $r = 0.89$ ) is not as strong as for As, Sb, and Zn because there is a slight but steady upcore decrease in the Mo/Fe ratio. Hence, although the upcore profile for Mo is fairly similar to that of Fe (and As, Sb, and Zn), other processes (e.g., removal; German et al., 1991) are affecting bulk Mo concentrations. In contrast, elements typically linked to the terrigenous fraction of sediment (Cr, Cs, Hf, Sc, and Th) are depleted in lowermost Unit III samples, and increase in concentration upcore (Table 4; Fig. 7). The bulk Ce-anomaly ranges from less than 0.15 in lowermost Unit III samples (>66.5 mcd) to values in excess of 1.0 above 58.5 mcd. This observation again is consistent with an upcore transition from predominantly hydrothermal to terrigenous deposition. Extremely low Ce/Ce\* values are characteristic of sediment deposited along flanks of active ridges, whereas very high Ce/Ce\* values (upwards of 1.6) typically are found in red clay sequences (Ruhlin and Owen, 1986; Toyoda et al., 1990; Murray et al., 1991).

All of the REEs (except Ce) are strongly intercorrelated ( $r > 0.93$ ), and their concentration profiles differ from those of elements associated with hydrothermal or terrigenous components (Fig. 8). The REE profiles display relatively low concentrations in lowermost samples, a pronounced peak at 66.5 mcd, and a gradual decline in concentration above 66.5 mcd. This pattern most likely arises from postdepositional REE scavenging by hydrothermal oxyhydroxide particulates (cf. Ruhlin and Owen, 1986; German et al., 1990; Olivarez and Owen, 1991). The concentration of a scavenged REE (except Ce) in distal hydrothermal sediment is proportional to two factors (Olivarez and Owen, 1991): the amount of primary hydrothermal component, and the time over which REE scavenging can occur. Lowermost Unit III samples are deficient in REEs because this sediment was rapidly deposited (relative to later samples) and did not have sufficient time to scavenge REEs. On the other hand, uppermost Unit III samples are depleted in REEs because this sediment lacks primary hydrothermal components. The prominent peak in REE concentrations at 66.5 mcd, therefore, represents the point at which these opposing effects are balanced (i.e., optimal conditions for maximum REE scavenging). Recognizing that variations in REE profiles (except Ce) reflect scavenging is of importance to this investigation inasmuch as it provides the background for one means of estimating hydrothermal accumulation through time.

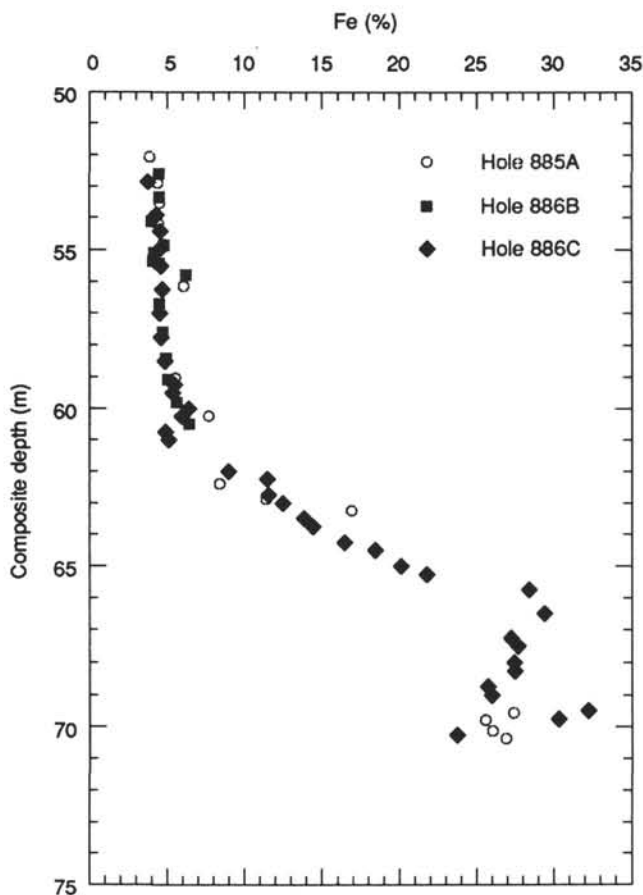


Figure 6. Bulk Fe concentration profile for samples from Unit III of Holes 885A, 886B, and 886C. Note the enrichment of Fe (>23 wt%) in samples below 66 mcd, the gradual decrease in Fe between 59 and 66 mcd, and the relatively low "background" values (4.5–5 wt%) above 59 mcd. Iron is considered representative of elements (As, Mo, Sb, and Zn) from the hydrothermal source.

### Hydrothermal Accumulation at Sites 885 and 886

Previous investigations have shown that the accumulation rate of distal hydrothermal materials decreases exponentially with increasing distance (or time) from the ridge axis (Boström et al., 1969; Dymond, 1981; Lyle et al., 1986; Marchig and Erzinger, 1986). Conventional techniques (e.g., examination of mass accumulation vs. time plots) cannot be used to determine if the hydrothermal component of Unit III sediment exhibits this characteristic profile because numerous and accurate age markers are lacking for this unit. However, this assessment can be made indirectly by employing modeling techniques and by using appropriate elemental concentrations as proxy indicators of the hydrothermal and terrigenous components. For example, if it is assumed that the flux of terrigenous material is constant, then it can be shown (Dickens and Owen, 1993) that:

$$MAR_H \propto \frac{C_H}{C_T}, \quad (1)$$

where  $MAR_H$  is the mass accumulation rate of the hydrothermal component, and  $C_H$  and  $C_T$  are the concentrations of elements that serve as proxies for the amounts of hydrothermal and terrigenous components in any sample. Within Unit III sediment, concentrations of As, Fe, Sb, and Zn are principally related to the distal hydrothermal component, and concentrations of Cr, Cs, Sc, and Th are primarily associated with the terrigenous component. Changes in the concentration ratio of any "hydrothermal element" (e.g., Fe) to any "terrigenous element" (e.g., Sc), therefore, should reflect variations in the

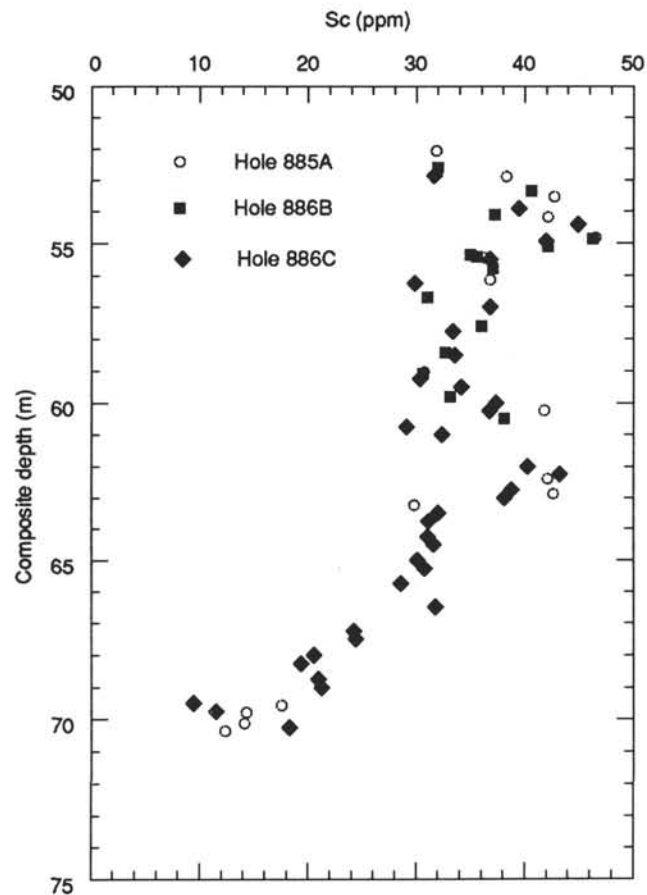


Figure 7. Bulk Sc concentration profile for samples from Unit III of Holes 885A, 886B, and 886C. Note that samples below 69 mcd are significantly depleted in Sc, and that values steadily increase between 63 and 69 mcd. Scandium is considered representative of elements (Cr, Cs, Hf, and Th) primarily associated with detrital materials.

enous element" (e.g., Sc), therefore, should reflect variations in the  $MAR$  of the distal hydrothermal component, provided the accumulation rate of the terrigenous component was relatively constant through time. The Fe/Sc ratio of samples from Unit III decreases in a roughly exponential pattern between 69.5 and 60 mcd (Fig. 9). Indeed, upcore variations in the Fe/Sc ratio between the above depths can be approximated by a simple exponential curve,  $Fe/Sc = Ae^{kd}$  ( $r > 0.90$ ), where  $k$  is a constant, and  $d$  is meters of composite depth (Dickens and Owen, 1993). Profiles of other "hydrothermal" to "terrigenous" elemental ratios are relatively similar to that of the Fe/Sc ratio, although it is difficult to compare all samples because concentrations of Cr, Cs, and Th are at or near detection limits in lowermost samples.

Because fluxes of terrigenous material (and therefore fluxes of Cr, Cs, Sc, and Th) can vary significantly over relatively short geologic time scales (e.g., Hovan et al., 1989), an alternative model that avoids the assumption of a constant flux of terrigenous material can be developed based upon considerations of REE scavenging (Dickens and Owen, 1993). This model is summarized as follows:

$$MAR_H \propto \frac{(C_H^2)(DBD)}{S_{REE}}, \quad (2)$$

where  $MAR_H$  is the mass accumulation rate of the distal hydrothermal component,  $C_H$  is defined as stated above,  $DBD$  is the dry bulk density, and  $S_{REE}$  is the amount of any REE that has been scavenged. This model assumes the sediment depth over which REEs are scavenged

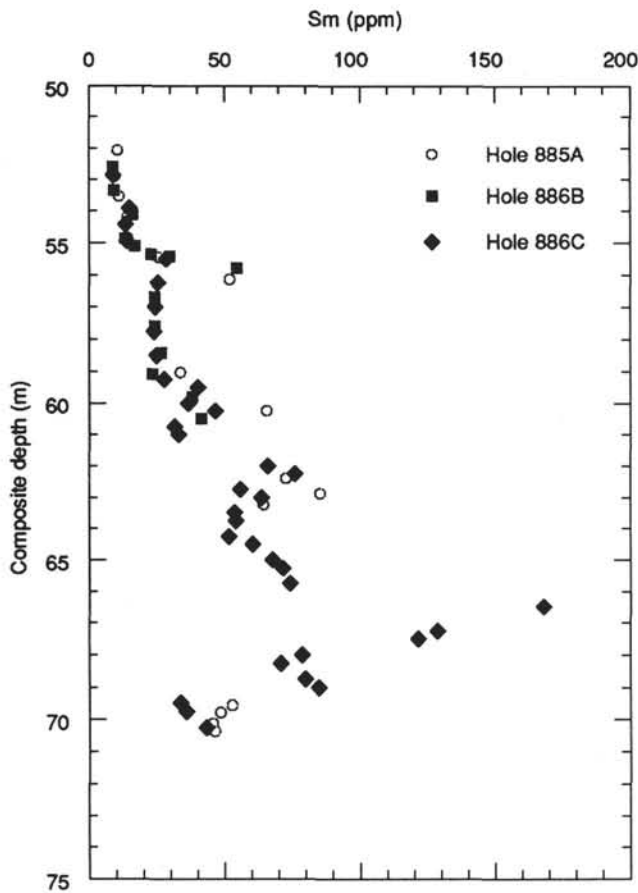


Figure 8. Bulk Sm concentration profile for samples from Unit III of Holes 885A, 886B, and 886C. Profiles for other REEs (except Ce) are very similar to that of Sm and display a relative depletion in lowermost and uppermost samples, but an enrichment between 62 and 68 mcd. This type of profile most likely results from postdepositional scavenging of REEs by hydrothermal oxyhydroxides.

is constant for all samples; however, variations in hydrothermal accumulation determined by this model are independent of assumptions regarding fluxes of other sedimentary components. The overwhelming amount of REEs in distal hydrothermal sediment are scavenged postdepositionally at or near the sediment/water interface (i.e., REEs are not "primary"; Olivarez and Owen, 1989; German et al., 1990), and depth profiles of REEs at Sites 885 and 886 indeed appear to reflect scavenging (Fig. 8). Hence, bulk REE concentrations may be used as a proxy for scavenged REE concentrations for samples from Unit III (i.e., bulk REE  $\approx S_{\text{REE}}$ ).

When concentrations of Fe and Sm are substituted into the above model, a roughly exponential decrease is observed between 69.5 and 60 mcd (Fig. 10). Profiles constructed by using other "hydrothermal" elements (e.g., As, Sb, and Zn) and REEs (other than Ce) are very similar to the one shown in Figure 10. Thus, either model suggests that accumulation of the distal hydrothermal component decreased in a roughly exponential pattern with respect to time between the middle Campanian and the early Paleogene. Deviations between the observed pattern and an expected exponential decrease may reflect variations in bottom-water flow, particle size distribution at vents, and/or intensity of hydrothermal activity (Lyle et al., 1986, 1987).

The Cretaceous/Tertiary (K/T) boundary has been located at 63.25 mcd in Unit III by anomalous Ir concentrations, shocked quartz, and strontium isotopic analyses of fish teeth (Kyte and Zhou, and Snoeckx et al., both this volume). The "tail-end" of the hydrothermal signal (~60 mcd), therefore, is slightly younger than 65.4 Ma. The presence of Unit IV basalt dictates the maximum lower age constraint: argon

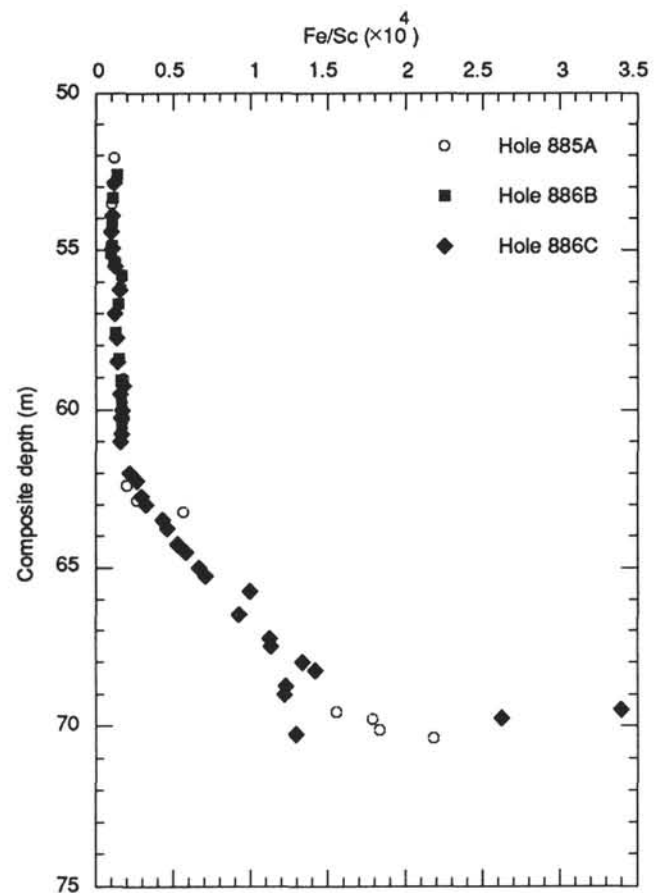


Figure 9. Hydrothermal accumulation through time according to Model 1 (text), given that Fe is primarily associated with the hydrothermal component and Sc is primarily associated with the terrigenous component.

argon dating indicates that the basalt underlying Unit III was emplaced at  $80 \pm 1.0$  Ma (Keller, this volume). Because Unit IV basalt lies approximately 80 m above basement, has glassy margins (at Site 885), and lacks characteristic baked contacts of a sill (Rea, Basov, Janecek, Palmer-Julson, et al., 1993), we interpret this basalt as a lava flow (i.e., we suggest that the Unit IV basalt is genetically related to rifting). The exponential decrease in hydrothermal accumulation (69.5–60 mcd), therefore, began after  $80 \pm 1.0$  Ma. If a hiatus (or interval of lower sedimentation rates) is not present in the lowest 1.4 m of Unit III sediment (i.e., between 69.5 mcd and Unit IV basalt), hydrothermal accumulation at Sites 885 and 886 was at a maximum at about 78–80 Ma. However, strontium isotopic analyses of fish teeth found in sediment at 69.7 and 70.1 mcd render ages of 74.5 and 76.5 Ma (Snoeckx et al., this volume). These ages suggest that the lowest 1.4 m of sediment was deposited at slower rates than immediately overlying sediment, and would place the maximum in hydrothermal accumulation at about 74 Ma. Although we cannot discriminate between these two possibilities with the information available, either scenario implies that deposition of distal hydrothermal material spanned at least 9 m.y. at Sites 885 and 886.

## CONCLUSIONS

The carbonate-free hydrothermal signal observed at Sites 885 and 886 is consistent with tectonic models concerning the origin of the Chinook Trough and can be explained as follows. During the early Late Cretaceous (>80 Ma), Sites 885 and 886 were located on the Farallon Plate at a depth beneath the CCD. Intraplate rifting (as evidenced by the Chinook Trough) then occurred at approximately 80

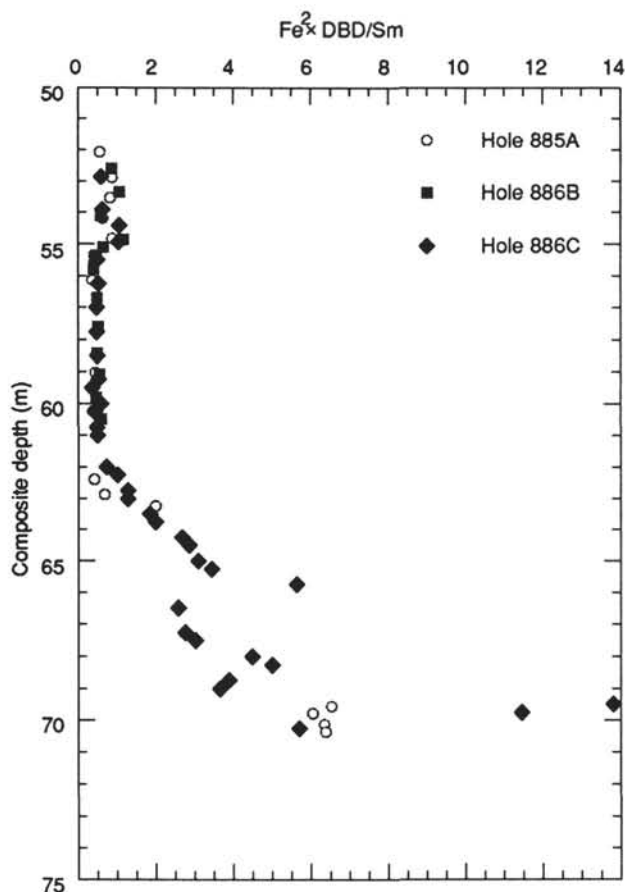


Figure 10. Hydrothermal accumulation through time according to Model 2 (text), given that Fe is primarily associated with the hydrothermal component, and all Sm has been scavenged at or near the sediment/water interface. Dry bulk density data used to calculate these values were extrapolated from index properties for Sites 885 and 886 (Rea, Basov, Janecek, Palmer-Julson, et al., 1993).

Ma and 60 km north of Sites 885 and 886. Effects of this rifting included creation of the Kula-Pacific spreading ridge, onset of north-south seafloor spreading, and initiation of hydrothermal activity (and possibly the eruption of basaltic lava flows). During the first stage of relatively slow seafloor spreading (~75–80 Ma), the Kula-Pacific Ridge was characterized by rough topography and a prominent axial valley. This may have been a time at which buoyant plumes could not escape the immediate vicinity of the Kula-Pacific Ridge (as perhaps indicated by ages determined from strontium isotopic analyses of fish teeth). At approximately 75 Ma, a tectonic change occurred such that topography along the Kula-Pacific spreading ridge was smoother and spreading rates were faster. Because Sites 885 and 886 were still proximal (within 150 km) to the Kula-Pacific spreading ridge at this time, deposition at Sites 885 and 886 was almost exclusively of hydrothermal precipitation from overlying neutrally buoyant plumes. As the ridge system matured, however, the distance between the Kula-Pacific spreading ridge and Sites 885 and 886 progressively increased such that hydrothermal accumulation decreased in a roughly exponential pattern. By the early Paleocene, this distance (Kula-Pacific spreading ridge to Sites 885 and 886) was of sufficient length (>600 km) that hydrothermal deposition was negligible.

#### ACKNOWLEDGMENTS

Funding for G.R. Dickens was supported by the U.S. Department of Energy under appointment to Graduate Fellowships for Global Change administered by Oak Ridge Institute for Science and Educa-

tion (ORISE). Cruise participation and research funding for R.M. Owen was supported by National Science Foundation (Texas A&M Research Foundation), award number USSSP 145-20682. We thank S. Dunn for her help in sample preparation, P. Simpson and E. Birdsall at the Phoenix Memorial Laboratory for aid in INAA, and D. Austin for processing our XRD patterns. T. Atwater, D.K. Rea, and attendees of the Leg 145 post-cruise meeting provided several suggestions during discussion of this work. C.L. Morgan and J.R. Moore contributed valuable comments based on a review of an earlier version of this paper.

#### REFERENCES\*

- Atwater, T., Sclater, J., Sandwell, D., Severinghaus, J., and Marlow, M.S., 1993. Fracture zone traces across the North Pacific Cretaceous Quiet Zone and their tectonic implications. In Pringle, M.S., Sager, W.W., Sliter, W.V., and Stein, S. (Eds.), *The Mesozoic Pacific: Geology, Tectonics, and Volcanism*. Geophys. Monogr., Am. Geophys. Union, 77:137–154.
- Baker, E.T., LaVelle, J.W., and Massoth, G.J., 1985. Hydrothermal particle plumes over the southern Juan de Fuca Ridge. *Nature*, 316:342–344.
- Barrett, T.J., Jarvis, I., Longstaffe, F.J., and Farquhar, R., 1988. Geochemical aspects of hydrothermal sediments in the eastern Pacific Ocean: an update. *Can. Mineral.*, 26:841–858.
- Barrett, T.J., Taylor, P.N., Jarvis, I., and Lugowski, J., 1986. Pb and Sr isotope and rare earth element composition of selected metalliferous sediments from Sites 597 to 601, Deep Sea Drilling Project Leg 92. In Leinen, M., Rea, D.K., et al., *Init. Repts. DSDP*, 92: Washington (U.S. Govt. Printing Office), 391–407.
- Boss, S.K., and Wilkinson, B.H., 1991. Planktonic/eustatic control on cratonic/oceanic carbonate accumulation. *J. Geol.*, 99:497–513.
- Boström, K., Peterson, M.N.A., Joensuu, O., and Fisher, D.E., 1969. Aluminum-poor ferromanganous sediments on active oceanic ridges. *J. Geophys. Res.*, 74:3261–3270.
- Browne, E., and Firestone, R.B., 1986. *Table of Radioactive Isotopes*: New York (Wiley).
- Cande, S.C., Herron, E.M., and Hall, B.R., 1982. The early Cenozoic tectonic history of the southeast Pacific. *Earth Planet. Sci. Lett.*, 57:63–74.
- Cande, S.C., and Kent, D.V., 1992. A new geomagnetic polarity time scale for the Late Cretaceous and Cenozoic. *J. Geophys. Res.*, 97:13917–13951.
- De Baar, H.J.W., German, C.R., Elderfield, H., and Van Gaans, P., 1987. Rare earth element distributions in anoxic waters of the Cariaco Trench. *Geochim. Cosmochim. Acta*, 52:1203–1219.
- Dehairs, F., Chesselet, R., and Jedwab, J., 1980. Discrete suspended particles of barite and the barium cycle in the open ocean. *Earth Planet. Sci. Lett.*, 49:528–550.
- Dickens, G.R., and Owen, R.M., 1993. Chinook Trough rifting and late Cretaceous hydrothermal deposition at ODP Site 886. *Eos*, 74:355.
- Dymond, J., 1981. Geochemistry of Nazca Plate surface sediments: an evaluation of hydrothermal, biogenic, detrital, and hydrogenous sources. In Kulm, L.D., Dymond, J., Dasch, E.J., Hussong, D.M., and Roderick, R. (Eds.), *Nazca Plate: Crustal Formation and Andean Convergence*. Mem.—Geol. Soc. Am., 154:133–173.
- Erickson, B.H., Rea, D.K., and Naugler, F.P., 1969. Chinook Trough: a probable consequence of north-south seafloor spreading. *Eos*, 50:633.
- Feely, R.A., Geiselman, T.L., Baker, E.T., and Massoth, G.J., 1990a. Distribution and composition of hydrothermal plume particles from the ASHES Vent Field at Axial Volcano, Juan de Fuca Ridge. *J. Geophys. Res.*, 95:12855–12873.
- Feely, R.A., Massoth, G.J., Baker, E.T., Cowen, J.P., Lamb, M.F., and Krogslund, K.A., 1990b. The effect of hydrothermal processes on mid-water phosphorous distributions in the northwest Pacific. *Earth Planet. Sci. Lett.*, 96:305–318.
- Fouquet, Y., Von Stackelberg, U., Charlou, J.L., Donval, J.P., Erzinger, J., Foucher, J.P., Herzig, P., Muehe, R., Soakai, S., Wiedicke, M., and Whitechurch, H., 1991. Hydrothermal activity and metallogenesis in the Lau back-arc basin. *Nature*, 349:778–781.
- Froelich, P.N., Klinkhammer, G.P., Bender, M.L., Luedtke, N.A., Heath, G.R., Cullen, D., Dauphin, P., Hammond, D., Hartman, B., and Maynard, V., 1979. Early oxidation of organic matter in pelagic sediments of the eastern

\* Abbreviations for names of organizations and publications in ODP reference lists follow the style given in *Chemical Abstracts Service Source Index* (published by American Chemical Society).

- equatorial Atlantic: suboxic diagenesis. *Geochim. Cosmochim. Acta*, 43:1075–1090.
- German, C.R., Campbell, A.C., and Edmond, J.M., 1991. Hydrothermal scavenging at the Mid-Atlantic Ridge: modification of trace element dissolved fluxes. *Earth Planet. Sci. Lett.*, 107:101–114.
- German, C.R., Klinkhammer, G.P., Edmond, J.M., Mitra, A., and Elderfield, H., 1990. Hydrothermal scavenging of rare earth elements in the ocean. *Nature*, 345:516–518.
- Gladney, E.S., O'Malley, B.T., Roelands, I., and Gills, T.E., 1987. Standard reference materials: compilation of elemental concentration data for NBS clinical, biological, geological, and environmental standard reference materials. *NBS Spec. Publ. (U.S.)*, 260–111.
- Honnorez, J., Von Herzen, R.P., et al., 1983. *Init. Repts. DSDP*, 70: Washington (U.S. Govt. Printing Office).
- Hovan, S.A., Rea, D.K., Piasias, N.G., and Shackleton, N.J., 1989. A direct link between the China loess and marine  $\delta^{18}\text{O}$  records: aeolian flux to the North Pacific. *Nature*, 340:296–298.
- Kennett, J.P., 1982. *Marine Geology*: Englewood Cliffs, NJ (Prentice-Hall).
- Klinkhammer, G., and Hudson, A., 1986. Dispersal patterns for hydrothermal plumes in the South Pacific using manganese as a tracer. *Earth Planet. Sci. Lett.*, 79:241–249.
- Kyte, F.T., Leinen, M., Heath, G.R., and Zhou, L., 1993. Cenozoic sedimentation history of the central North Pacific: inferences from the elemental geochemistry of Core LL44-GPC3. *Geochim. Cosmochim. Acta*, 57:1719–1740.
- Lupton, J.E., Klinkhammer, G.P., Normack, W.R., Hagman, R., MacDonald, K.C., Weiss, R.F., and Craig, H., 1981. Helium-3 and manganese at the 21°N East Pacific Rise hydrothermal site. *Earth Planet. Sci. Lett.*, 50:115–127.
- Lyle, M., Leinen, M., Owen, R.M., and Rea, D.K., 1987. Late Tertiary history of hydrothermal deposition at the East Pacific Rise, 19°S: correlation to volcano-tectonic events. *Geophys. Res. Lett.*, 14:595–598.
- Lyle, M., Owen, R.M., and Leinen, M., 1986. History of hydrothermal sedimentation at the East Pacific Rise, 19°S. In Leinen, M., Rea, D.K., et al., *Init. Repts. DSDP*, 92: Washington (U.S. Govt. Printing Office), 585–596.
- Mammerickx, J., and Sharman, G.F., 1988. Tectonic evolution of the North Pacific during the Cretaceous quiet period. *J. Geophys. Res.*, 93:3009–3024.
- Marchig, V., and Erzinger, J., 1986. Chemical composition of Pacific sediments near 20°S: changes with increasing distance from the East Pacific Rise. In Leinen, M., Rea, D.K., et al., *Init. Repts. DSDP*, 92: Washington (U.S. Govt. Printing Office), 371–381.
- Meylan, M.A., Glasby, G.P., Knedler, K.E., and Johnston, J.H., 1981. Metalliferous deep-sea sediments. In Wolf, K.H. (Ed.), *Handbook of Stratiform and Stratiform Ore Deposits* (Vol. 9): Amsterdam (Elsevier), 77–178.
- Michard, A., Albarede, F., Michard, G., Minster, J.F., and Charlou, J.L., 1983. Rare earth elements and uranium in high-temperature solutions from East Pacific Rise hydrothermal vent field (13°N). *Nature*, 303:795–797.
- Murray, R.W., Ten Brink, M.R.B., Gerlach, D.C., Russ, G.P., III, and Jones, D.L., 1991. Rare earth, major, and trace elements in chert from the Franciscan Complex and Monterey Group, California: assessing REE sources to fine-grained marine sediments. *Geochim. Cosmochim. Acta*, 55:1875–1895.
- Olivarez, A.M., and Owen, R.M., 1991. The europium anomaly of seawater: implications for fluvial versus hydrothermal REE inputs to the oceans. *Chem. Geol.*, 92:317–328.
- Owen, R.M., and Rea, D.K., 1985. Sea-floor hydrothermal activity links climate to tectonics: the Eocene CO<sub>2</sub> greenhouse. *Science*, 227:166–169.
- Owen, R.M., and Ruhlin, D.E., 1986. Interlaboratory comparison of Leg 92 standard sediment sample analyses. In Leinen, M., Rea, D.K., et al., *Init. Repts. DSDP*, 92: Washington (U.S. Govt. Printing Office), 353–354.
- Owen, R.M., and Zimmerman, A.R.B., 1991. Geochemistry of Broken Ridge sediments. In Weissel, J., Peirce, J., Taylor, E., Alt, J., et al., *Proc. ODP. Sci. Results*, 121: College Station, TX (Ocean Drilling Program), 437–445.
- Piper, D.Z., 1974. Rare earth elements in the sedimentary cycle: a summary. *Chem. Geol.*, 14:285–304.
- Rabouille, C., and Gaillard, J.-F., 1991. Towards the EDGE: early diagenetic global explanation: a model depicting the early diagenesis of organic matter, O<sub>2</sub>, NO<sub>3</sub>, Mn and PO<sub>4</sub>. *Geochim. Cosmochim. Acta*, 55:2511–2525.
- Rea, D.K., 1970. Changes in structure and trend of fracture zones north of the Hawaiian Ridge and relation to seafloor spreading. *J. Geophys. Res.*, 75:1421–1430.
- , 1981. Tectonics of the Nazca-Pacific divergent plate boundary. In Kulm, L.D., Dymond, J., Dasch, E.J., and Hussong, E.M. (Eds.), *Nazca Plate: Crustal Formation and Andean Convergence*. Mem.—Geol. Soc. Am., 154:27–62.
- Rea, D.K., Basov, I.A., Janecek, T.R., Palmer-Julson, A., et al., 1993. *Proc. ODP. Init. Repts.*, 145: College Station, TX (Ocean Drilling Program).
- Rea, D.K., and Dixon, J.M., 1983. Late Cretaceous and Paleogene tectonic evolution of the North Pacific Ocean. *Earth Planet. Sci. Lett.*, 65:145–166.
- Rea, D.K., and Duncan, R.A., 1986. North Pacific Plate convergence: a quantitative record of the past 140 m.y. *Geology*, 14:373–376.
- Rea, D.K., and Leinen, M., 1986. Crustal subsidence and calcite deposition in the South Pacific Ocean. In Leinen, M., Rea, D.K., et al., *Init. Repts. DSDP*, 92: Washington (U.S. Govt. Printing Office), 299–303.
- Renkin, M.L., and Sclater, J.G., 1988. Depth and age in the North Pacific. *J. Geophys. Res.*, 93:2919–2935.
- Ruhlin, D.E., and Owen, R.M., 1986. Factors influencing the rare earth element composition of hydrothermal precipitates, East Pacific Rise. In Leinen, M., Rea, D.K., et al., *Init. Repts. DSDP*, 92: Washington (U.S. Govt. Printing Office), 383–389.
- Sclater, J.G., Anderson, R.N., and Bell, M.L., 1971. Elevation of ridges and evolution of the central eastern Pacific. *J. Geophys. Res.*, 76:7888–7915.
- Sengör, A.H.C., and Burke, K., 1978. Relative timing of rifting and volcanism on Earth and its tectonic implications. *Geophys. Res. Lett.*, 5:419–421.
- Toyoda, K., Nakamura, Y., and Masuda, A., 1990. Rare earth elements of Pacific pelagic sediments. *Geochim. Cosmochim. Acta*, 54:1093–1103.
- Van Andel, T.H., 1975. Mesozoic/Cenozoic calcite compensation depth and the global distribution of calcareous sediments. *Earth Planet. Sci. Lett.*, 26:187–194.
- Von Damm, K.L., Edmond, J.M., Grant, B., Measures, C.I., Walden, B., and Weiss, R.F., 1985. Chemistry of submarine hydrothermal solutions at 21°N, East Pacific Rise. *Geochim. Cosmochim. Acta*, 49:2197–2220.
- Woods, M.T., and Davies, G.F., 1982. Late Cretaceous genesis of the Kula Plate. *Earth Planet. Sci. Lett.*, 58:161–166.

**Date of initial receipt: 4 April 1994**

**Date of acceptance: 23 June 1994**

**Ms 145SR-128**

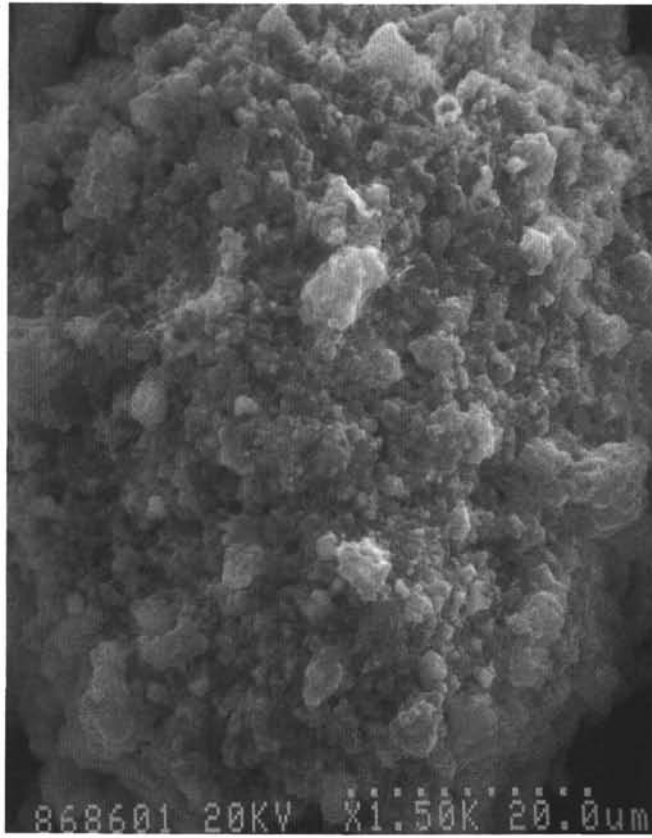


Plate 1. An apatite concretion from Sample 145-886C-8H-6, 80 cm.